

# Large-Scale Quantum Network over 66 Orbital Angular Momentum Optical Modes

Wei Wang,<sup>1</sup> Kai Zhang,<sup>1</sup> and Jietai Jing<sup>1,2,3,\*</sup>

<sup>1</sup>*State Key Laboratory of Precision Spectroscopy, Joint Institute of Advanced Science and Technology, School of Physics and Electronic Science, East China Normal University, Shanghai 200062, China*

<sup>2</sup>*Department of Physics, Zhejiang University, Hangzhou 310027, China*

<sup>3</sup>*Collaborative Innovation Center of Extreme Optics, Shanxi University, Taiyuan, Shanxi 030006, China*



(Received 3 March 2020; revised 6 August 2020; accepted 14 September 2020; published 1 October 2020)

Multipartite entanglement (ME) is the fundamental ingredient for building quantum networks. The scale of ME determines its quantum information carrying and processing capability. Most of the current efforts for boosting the scale of ME focus on increasing the number of entangled nodes. However, the number of channels for broadcasting ME is also an important index for characterizing its scale. In this Letter, we experimentally exploit orbital angular momentum multiplexing and the spatial pump shaping technique to simultaneously and deterministically generate 11 channels of individually accessible and mutually orthogonal continuous variable (CV) spatially separated hexapartite entangled states over 66 optical modes in a single quantum system. These results suggest that our method can greatly expand the scale of ME and provide a new perspective and platform to construct a CV quantum network.

DOI: 10.1103/PhysRevLett.125.140501

For constructing quantum networks [1], such as multi-user quantum teleportation [2] and dense coding [3], multipartite entanglement (ME) is an indispensable physical resource. The performance of ME in the respect of information capacity is largely determined by its scale, which depends not only on the number of involved parties or entangled nodes, but also on the number of channels for broadcasting the ME. If multiple channels of independent and orthogonal ME can exist simultaneously, i.e., be multiplexed, the channel capacity of the quantum network will be greatly enhanced.

There are two equally important routes for constructing a quantum information network, namely, the discrete variable (DV) [4–6] and continuous variable (CV) [7] systems. For building large-scale quantum networks, these two routes have their own advantages and disadvantages in terms of both scalability and transmission distance. The transmission distance of the DV system can be increased relatively easily [8–10] since DV entanglement is not sensitive to optical losses. Its scale can be enhanced by increasing either the dimensionality of the state [11–16] or the number of entanglement degrees of freedom (DOFs) [17–19] without significantly reducing the detection rate. To increase the number of entangled photons [20–22] is challenging due to the probabilistic generation of DV entanglement. Because of the deterministic generation of CV entanglement, the scale of the CV system can be enhanced relatively easily by increasing either the number of the entangled modes [23,24] or the number of the multiplexed channels [25]. To increase the transmission distance for a CV system is challenging since the CV entanglement is sensitive to optical losses. Our work here

focuses on the CV system. Traditionally, the generation of CV ME is based on successive beam splitting processes [26,27]. In order to increase the scale of the CV system, the current trend is to integrate multiple nonlinear processes into a single device using the frequency, temporal, or time properties of the light field [23,24,28–31]. These schemes are particularly useful for measurement-based quantum computing by exploiting the spatially colocated large-scale cluster states. For realizing distant high-capacity quantum communication, large-scale ME with its modes spatially separated is required. The purpose of our work here is to efficiently engineer such large-scale ME.

Recently, the orbital angular momentum (OAM) of the light field, one of the most fundamental physical quantities, has been used to realize multiplexing [32–34] in classical communication due to the infinite range of possibly achievable OAM space. Because of that, it has been studied deeply in DV [6] quantum systems, such as the generation of high-dimensional DV two-photon [11] and multiphoton [13] quantum entanglement, the quantum teleportation of multiple DOFs of a single photon [35], the generation of DV quantum entanglement in multiple DOFs [18], narrow-band hyperentanglement [36], and entanglement swapping of multiple OAM states of light [37]. Compared with its in-depth study in the DV quantum system, OAM finds only a few applications in CV [7] quantum systems, including the generation of low-order OAM modes [38,39]. Very recently, OAM multiplexed CV bipartite [25] and tripartite [40] entanglement have been experimentally demonstrated, showing that OAM multiplexing is an effective way to boost the scale of entanglement. In this Letter, we exploit the spatial pump shaping (SPS) technique to increase the

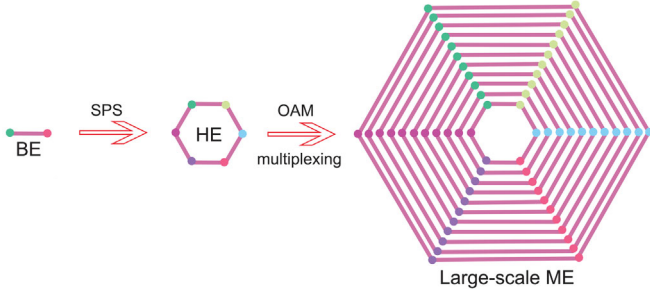


FIG. 1. The principle for engineering large-scale ME. The initial state is a bipartite entanglement (BE). By the spatial pump shaping technique, the number of the entangled parties increases to 6, forming a hexapartite entanglement. Then with orbital angular momentum multiplexing, the number of the multiplexed channels increases to 11, leading to the generation of large-scale ME over 66 OAM optical modes.

number of the parties of the spatially separated ME ( $M$ ) and utilize OAM multiplexing to increase the number of the channels for broadcasting the ME ( $N$ ). As a result, our method increases the scale of the ME to  $M \times N$ , showing its great advantage for efficiently engineering large-scale spatially separated ME.

The principle of our scheme is depicted in Fig. 1. The four-wave mixing (FWM) process in a hot atomic vapor cell has been proved as a promising candidate to produce bipartite entanglement [41]. By using the SPS technique to

generate seven concurrent FWM processes in a single cell [42], we could deterministically generate a CV hexapartite entanglement (HE). Then, in order to largely increase the scale of the prepared HE, we utilize the concept of OAM multiplexing. In particular, each party of the HE can have 11 possible individually accessible and mutually orthogonal OAM modes while maintaining the HE under certain experimental conditions as described below. Consequently, we can deterministically implement a large-scale ME by simultaneously generating 11 channels of hexapartite entangled states over 66 OAM modes.

The experimental setup is shown in Fig. 2(a). From a Ti: sapphire laser tuned about 0.8 GHz to the blue of the  $^{85}\text{Rb}$  D1 line transition ( $5\text{S}_{1/2}, F = 2 \rightarrow 5\text{P}_{1/2}$ ), two pump beams ( $\text{pump}_1$  and  $\text{pump}_2$ ) are generated. Then they are crossed at an angle of 8 mrad in the center of the cell. A weak Gaussian probe beam [5 in Fig. 2(a)], 3.04 GHz redshifted from the pump beam, is generated by double passing part of the pump beam through an acousto-optic modulator. After that, it is directed onto a spatial light modulator (SLM), which loads computer-generated hologram. In this way, the initial Gaussian beam becomes a Laguerre-Gauss (LG) beam with a topological charge of  $\ell$  dependent on the corresponding computer-generated hologram. The generated LG beam is symmetrically crossed with the two pump beams at an angle of about 5.7 mrad. The waists of the individual pump beam and Gaussian probe beam ( $\ell = 0$ ) are 1420 and 1090  $\mu\text{m}$ , respectively.

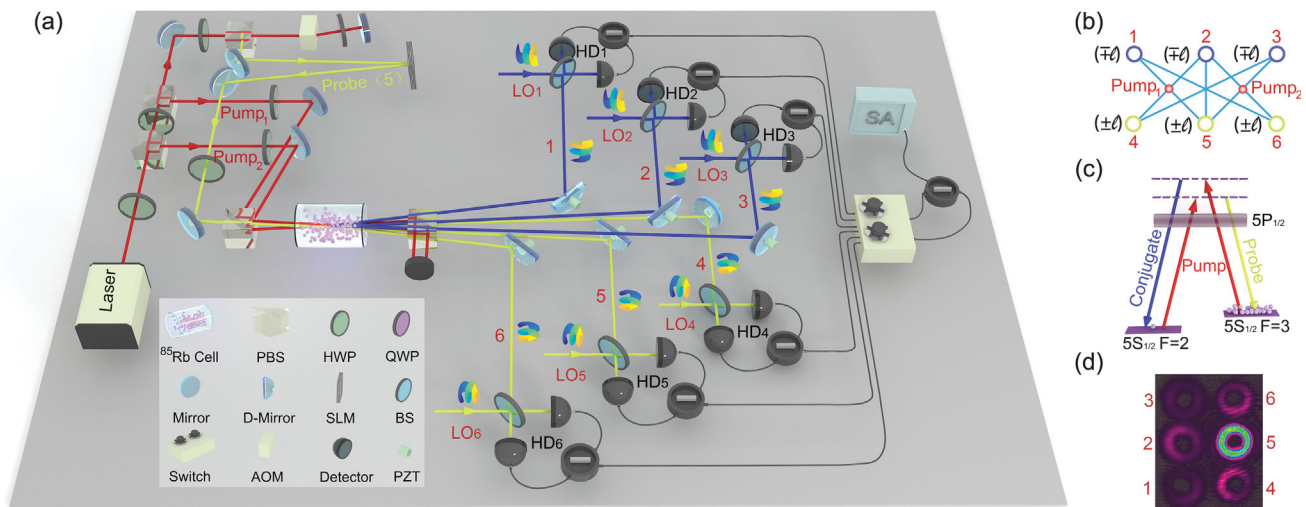


FIG. 2. Schematic of generating and detecting the large-scale ME. (a) The seven concurrent FWM processes happen in a  $^{85}\text{Rb}$  cell and the generated OAM multiplexed hexapartite states (beams 1 to 6) from it are detected by six homodyne detections (HDs). Pump<sub>1</sub> and pump<sub>2</sub> are intense pump beams. 1, 2, 3 denote conjugate beams while 4, 5, 6 denote probe beams. The injected probe beam coincides with beam 5. LO<sub>*i*</sub> (*i* = 1, 2, 3, 4, 5, 6) is the local oscillator for the corresponding HD<sub>*i*</sub>. Two home-made single pole six-throw switches (Switch) allow us to select any two of the photocurrents from the six HDs and to measure the correlation between their quadrature components by spectrum analyzer (SA). Polarization beam splitter (PBS), half wave plate (HWP), quarter wave plate (QWP), high reflectivity mirror (Mirror), D shaped mirror (D-Mirror), acousto-optic modulator (AOM), spatial light modulator (SLM), beam splitter (BS), piezo-electric transducer (PZT) which is used to scan the phase between signal light and LO. (b) Interaction structure of the six LG beams. (c) Double-A energy level configuration of the FWM process. (d) The camera-captured intensity pattern of six OAM modes when the topological charge of the injected probe beam 5 is 5.

Under this condition, seven concurrent FWM processes occur in the same cell as shown in Fig. 2(b). Each process follows a double- $\Lambda$  energy level configuration as shown in Fig. 2(c). First of all, the probe beam can interact with each pump beam via the normal single-pump FWM process [41]. The probe beam is amplified and two conjugate beams (1 and 3) are simultaneously generated. Then, in addition to the case of a single pump, the probe beam can also interact with both of the two pump beams as long as the phase matching condition is satisfied. In such a dual-pump case, each pump beam annihilates one photon, the probe beam gets one photon and another photon is generated synchronously in a new conjugate beam (2). In the meantime, the new probe beam 4 (6) is generated by the single-pump interaction between beam 2 and pump<sub>1</sub> (pump<sub>2</sub>) or the dual-pump interaction between beam 3 (1) and both of the two pump beams. As a result, the probe beam (5) is amplified while two new probe beams (4 and 6) and three conjugate beams (1, 2, and 3) are generated. Because the injected probe beam 5 is LG beam carrying OAM, the six output beams will also carry OAM. Because of OAM conservation [25], the topological charges of the generated three probe beams and three conjugate beams are opposite. Consequently, if we vary the topological charge  $\ell$  of the probe beam 5, we can get multiple channels of HE, in which each party carries OAM mode. Since the different OAM modes are orthogonal with each other, the different channels of HE will be also mutually orthogonal. This makes each channel of HE individually accessible. Figure 2(d) shows the camera-captured intensity pattern of the six output beams when the injected probe beam is LG<sub>5</sub>, i.e., OAM mode with topological charge of 5. Such seven concurrent FWM processes with bright seeding imply the interaction structure of the generated beams and benefit to the experimental alignment. But when testing entanglement, the seeded probe beam 5 is blocked, making the measured processes purely spontaneous.

Note that the OAM modes in single probe or conjugate beam copropagate with each other. Therefore, in order to testify the quantum entanglement within one channel of six OAM modes, we have to first extract the specific OAM mode from its entire beam. To this end, we exploit the balanced homodyne detection (HD) technique with local oscillator (LO), which is a widely used method to extract mode and testify quantum entanglement in CV system. The six LOs are obtained by setting up a similar setup with a bright OAM-carrying probe seeded a few mm above the previous seven spontaneous FWM processes. In this way, the six derived LOs are LG beams carrying OAM. Then, by projecting the entire signal beam onto an OAM-carrying LO, we can extract the desired OAM mode and measure its quantum property. In such multi-spatial-mode FWM system, imperfect HD visibility can couple in uncorrelated amplified modes and largely deteriorate the entanglement

[43]. Therefore, it is critical to optimize the visibilities and here we achieve visibilities of about 95% for all the multiplexed channels. Compared with the most commonly used method for selecting the desired OAM states in DV system, which uses mode selectors consisting of computer-generated holograms and mono-mode optical fibers [11], the HD exploited here has much higher mode extraction efficiency and thus less introduced losses.

Quantum properties of any Gaussian states can be characterized by their second-order momenta, which can be conveniently organized in the form of a covariance matrix (CM) [44]. The HDs with LOs mode matched to the six signal fields under interrogation can get fluctuations of amplitude  $\hat{x}$  and phase  $\hat{p}$  quadratures of the six signal fields. Here, we use six individual HDs to get the full CM for each channel of HE (See Supplemental Material for details [45]). Based on the measured CM, the entanglement for each channel of six OAM modes can be certified with the positivity under partial transposition (PPT) criterion [49,50], which is stated in terms of the symplectic eigenvalues of the partially transposed (PT) CM [44]. There are three possible types of PT operations of  $1 \times 5$ ,  $2 \times 4$ , and  $3 \times 3$  for hexapartite scenario, which results in 31 possible bipartitions. The six OAM modes are entangled if all the symplectic eigenvalues are smaller than 1. In addition, a smaller eigenvalue implies a stronger entanglement [51].

To test the entanglement property of the large-scale ME, we measure the CM for the cases where the topological charge  $\ell$  of the injected probe for generating LOs is ranging from  $-5$  to  $5$ . Further increasing  $|\ell|$  is limited by the spatial overlap among the six OAM modes, making it hard to separate and measure them. Both pump<sub>1</sub> and pump<sub>2</sub> are set to 100 mW. Figures 3(a) and 3(b) show the 31 symplectic eigenvalues for the cases with different integer topological charge  $\ell$  in the range of  $-5$  to  $5$ . We can see that all the symplectic eigenvalues for the case of each topological

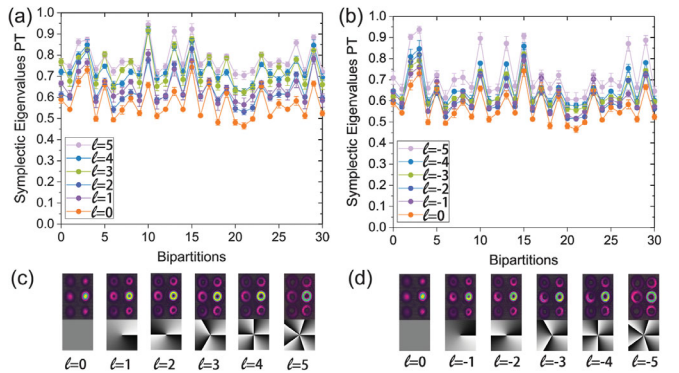


FIG. 3. Witnessing the large-scale ME. (a)–(b) All 31 bipartitions possess an eigenvalue below 1 for different cases of the topological charge  $\ell$  ( $\ell = -5$  to  $5$ ), indicating complete inseparability for the six OAM modes in each case. (c)–(d), The corresponding computer-generated holograms loaded on the SLM and the intensity patterns of the six LG beams.

charge  $\ell$  are smaller than 1, clearly demonstrating the presence of 11 channels of OAM multiplexed HE. Meanwhile, we can also find that the higher the  $|\ell|$  is, the larger the corresponding symplectic eigenvalues will be, showing a weaker entanglement. This is due to the fact that the beam size of the OAM mode increases with the increase of the  $|\ell|$ . Such beam-size increase will reduce the overlap and thus the interaction strength between the OAM mode and the pump beams. When the absolute value of the topological charge  $|\ell| = 1, 2, 3, 4$ , and 5, the waists of the seeded probe beam are 1110, 1160, 1220, 1300, and 1400  $\mu\text{m}$ , respectively. Figures 3(c) and 3(d) show the computer-generated holograms loaded on SLM and the corresponding intensity patterns of the six OAM modes when the probe beam 5 is on. It can be seen that the beam size of the six OAM modes in each case are all the same. This is because that their  $|\ell|$  are equal. For the corresponding topological charge verification of these output OAM modes, one can refer to the Supplemental Material [45], which clearly indicates the OAM conservation in this system.

So far, we have studied the OAM multiplexed large-scale ME carrying OAM modes with integer topological charge. It will be also interesting to study the HE for the case of coherent OAM superposition modes. Such HE of coherent OAM superposition modes have the potential to increase the transmission stability [52] and channel capacity [53] under practical turbulence conditions, and thus are useful for practical quantum communication. To this end, we load a more complex computer-generated hologram onto the SLM for generating coherent OAM superposition modes as LO beams. First, we study the cases where the injected probes for generating LOs are the coherent OAM superposition mode  $\text{LG}_1 + \text{LG}_{-1}$ ,  $\text{LG}_2 + \text{LG}_{-2}$ ,  $\text{LG}_3 + \text{LG}_{-3}$ ,  $\text{LG}_4 + \text{LG}_{-4}$ ,  $\text{LG}_5 + \text{LG}_{-5}$ , respectively.

The 31 symplectic eigenvalues for these cases of different coherent OAM superposition mode are shown in Fig. 4(a). They are all smaller than 1, indicating that there exist HE in these five cases. It can be found that the overall 31 symplectic eigenvalues increase with the increase of  $|\ell|$ . This is consistent with the results of Fig. 3. Second, we study the case of  $\sqrt{\kappa}\text{LG}_{-1} + \sqrt{1-\kappa}\text{LG}_{-3}$  modes.  $\kappa$  is gradually increased from 0 to 1 at intervals of 0.2. The 31 symplectic eigenvalues in these six different cases of  $\kappa$  are shown in Fig. 4(b). We can find that all the symplectic eigenvalues are smaller than 1 in these six cases, indicating the presence of HE. Third, we study the cases of  $\text{LG}_{-1} + e^{2i\theta}\text{LG}_1$ .  $\theta$  is gradually increased from  $0^\circ$  to  $360^\circ$  at intervals of  $90^\circ$ . When  $\theta$  is  $360^\circ$ , the mode returns to the initial one with  $\theta = 0^\circ$ . The 31 symplectic eigenvalues for these five different cases are shown in Fig. 4(c). It can also be seen that they are all smaller than 1 and are almost constant for  $\theta$  varying from  $0^\circ$  to  $360^\circ$ , which demonstrates the existence of HE in these cases. Figures 4(d), 4(e), and 4(f) are the computer-generated holograms of coherent OAM superposition modes loaded on SLM and the intensity patterns of the six entangled OAM superposition modes, corresponding to Fig. 4(a), Fig. 4(b), and Fig. 4(c), respectively.

The states studied here belong to large-scale ME for building quantum communication network while cluster states are preferred for measurement-based quantum computing [28,29]. Therefore, it is also interesting to explore the possibilities of using such FWM processes in hot atomic vapor to generate a large-scale cluster state. Two possibilities can be conceived. One possibility is the parallel generation of multiple sets of independent hexagon cluster states in OAM space by rotating three of the six modes by  $\pi/2$  analogy with the one in the frequency domain [28]. Another possibility is to produce dual-rail

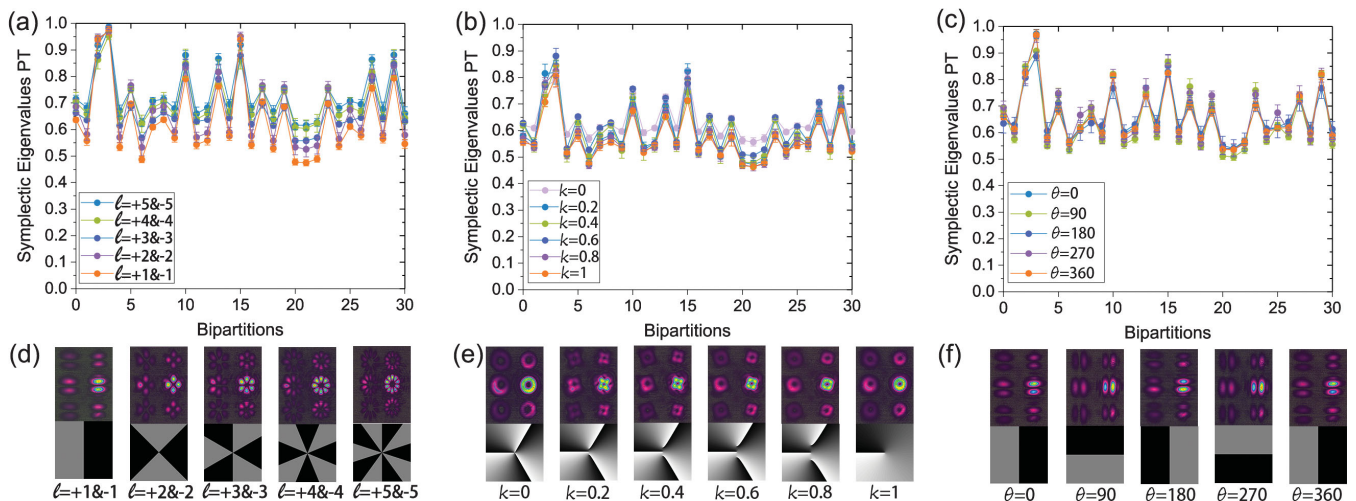


FIG. 4. Witnessing the HE for three types of coherent OAM superposition modes. The PPT test of HE for (a),  $\text{LG}_\ell + \text{LG}_{-\ell}$  modes. (b),  $\sqrt{\kappa}\text{LG}_{-1} + \sqrt{1-\kappa}\text{LG}_{-3}$  modes. (c),  $\text{LG}_{-1} + e^{2i\theta}\text{LG}_1$  modes. (d)-(f), The corresponding computer-generated holograms loaded on SLM and the intensity patterns of the six LG beams.

cluster state in OAM space by mixing two sets of independent FWM processes analogy with another work in frequency domain [29]. The cluster states proposed above are in OAM space while the cluster states in previous works [28,29] are in frequency domain. Such difference determines the challenges and advantages of each approach. For example, in principle, the dimensionality of OAM basis is infinite, making our approach as an alternative way to generate large-scale cluster state in addition to the methods of frequency [28,29] and time domains [23,24]. In order to do so, the challenge of our approach is to increase the spiral bandwidth of the FWM process. For the cluster states in frequency domain [28,29,54–57], the big advantage is their scalability to ultra-large-scale cluster state due to the huge phase matching bandwidth of their quantum optical frequency comb. The challenge of their scheme is the measurement of all the available modes.

In conclusion, we have experimentally demonstrated the deterministic generation of large-scale ME in the CV regime. In particular, through the exploiting of OAM multiplexing and SPS technique, we have experimentally implemented the simultaneous generation of 11 independent channels of spatially separated HE over 66 OAM modes. In addition, we also investigate the HE properties for three types of coherent OAM superposition modes. The present experimental results suggest that our method can greatly expand the scale of ME and provide a new perspective and platform to construct a large-scale quantum network. There are still several possibilities to further increase the scalability of our scheme, including increasing the number [58] and the waist [25] of the pump beams, reducing the length of the cell [59]. Integrating more DOFs with the current scheme, such as radial index and frequency of the optical modes, can also greatly enhance the scale of the system. By utilizing the OAM sorting technique [60], all the 66 involved modes can be spatially separated and independently accessed, making it particularly useful for building distant large-scale quantum communication networks. Recently, the integrated quantum optical platforms have shown great potential for quantum information processing due to their advantages of being compact, scalable, and stable [15,22,61–64]. Therefore, combining our scheme with an integrated optical platform may provide an alternative promising way for building a large-scale on-chip quantum network.

This work was funded by the National Natural Science Foundation of China (NSFC) (Grants No. 11874155, No. 91436211, No. 11374104, and No. 10974057), the Basic Research Project of Shanghai Science and Technology Commission (20JC1416100), the Natural Science Foundation of Shanghai (Grant No. 17ZR1442900), the Minhang Leading Talents (Grant No. 201971), the Program of Scientific and Technological Innovation of Shanghai (Grant No. 17JC1400401), the

National Basic Research Program of China (Grant No. 2016YFA0302103), Shanghai Municipal Science and Technology Major Project (Grant No. 2019SHZDZX01), the 111 project (Grant No. B12024), the Fundamental Research Funds for the Central Universities, ECNU Academic Innovation Promotion Program for Excellent Doctoral Students (Grant No. YBNL TS2019-012).

W. W and K. Z contributed equally to this work.

\*Corresponding author.

jting@phy.ecnu.edu.cn

- [1] H. J. Kimble, *Nature (London)* **453**, 1023 (2008).
- [2] H. Yonezawa, T. Aoki, and A. Furusawa, *Nature (London)* **431**, 430 (2004).
- [3] J. Jing, J. Zhang, Y. Yan, F. Zhao, C. Xie, and K. Peng, *Phys. Rev. Lett.* **90**, 167903 (2003).
- [4] D. R. Hamel, L. K. Shalm, H. Hubel, A. J. Miller, F. Marsili, V. B. Verma, R. P. Mirin, S. Nam, K. J. Resch, and T. Jennewein, *Nat. Photonics* **8**, 801 (2014).
- [5] Y. Pu, Y. Wu, N. Jiang, W. Chang, C. Li, S. Zhang, and L. Duan, *Sci. Adv.* **4**, eaar3931 (2018).
- [6] J.-W. Pan, Z. B. Chen, C. Y. Lu, H. Weinfurter, A. Zeilinger, and M. Żukowski, *Rev. Mod. Phys.* **84**, 777 (2012).
- [7] S. L. Braunstein and P. van Loock, *Rev. Mod. Phys.* **77**, 513 (2005).
- [8] S. Liao *et al.*, *Nature (London)* **549**, 43 (2017).
- [9] J. Yin *et al.*, *Science* **356**, 1140 (2017).
- [10] J. Yin *et al.*, *Nature (London)* **582**, 501 (2020).
- [11] A. Mair, A. Vaziri, G. Weihs, and A. Zeilinger, *Nature (London)* **412**, 313 (2001).
- [12] A. C. Data, J. Leach, G. S. Buller, M. J. Padgett, and E. Andersson, *Nat. Phys.* **7**, 677 (2011).
- [13] M. Malik, M. Erhard, M. Huber, M. Krenn, R. Fickler, and A. Zeilinger, *Nat. Photonics* **10**, 248 (2016).
- [14] D. Ding, W. Zhang, S. Shi, Z. Zhou, Y. Li, B. Shi, and G. Guo, *Light Sci. Appl.* **5**, e16157 (2016).
- [15] M. Kues, C. Reimer, P. Roztocki, L. R. Corts, S. Sciara, B. Wetzel, Y. Zhang, A. Cino, S. T. Chu, B. E. Little, D. J. Moss, L. Caspani, J. Azaña, and R. Morandotti, *Nature (London)* **546**, 622 (2017).
- [16] Y. Zhang, F. S. Roux, T. Konrad, M. Agnew, J. Leach, and A. Forbes, *Sci. Adv.* **2**, e1501165 (2016).
- [17] X. L. Wang, Y. H. Luo, H. L. Huang, M. C. Chen, Z. E. Su, C. Liu, C. Chen, W. Li, Y. Q. Fang, X. Jiang, J. Zhang, L. Li, N. L. Liu, C. Y. Lu, and J.-W. Pan, *Phys. Rev. Lett.* **120**, 260502 (2018).
- [18] W. Zhang, D. Ding, M. Dong, S. Shi, K. Wang, S. Liu, Y. Li, Z. Zhou, B. Shi, and G. Guo, *Nat. Commun.* **7**, 13514 (2016).
- [19] C. Reimer, S. Sciara, P. Roztocki, M. Islam, L. R. Cortés, Y. Zhang, B. Fisher, S. Loranger, R. Kashyap, A. Cino, S. T. Chu, B. E. Little, D. J. Moss, L. Caspani, W. J. Munro, J. Azaña, M. Kues, and R. Morandotti, *Nat. Phys.* **15**, 148 (2019).
- [20] H. S. Zhong, Y. Li, W. Li, L. C. Peng, Z. E. Su, Y. Hu, Y. M. He, X. Ding, W. Zhang, H. Li, L. Zhang, Z. Wang, L. You,

- X. L. Wang, X. Jiang, L. Li, Y. A. Chen, N. L. Liu, C. Y. Lu, and J.-W. Pan, *Phys. Rev. Lett.* **121**, 250505 (2018).
- [21] Y. Huang, B. Liu, L. Peng, Y. Li, L. Li, C. Li, and G. Guo, *Nat. Commun.* **2**, 546 (2011).
- [22] C. Reimer, M. Kues, P. Roztocki, B. Wetzel, F. Grazioso, B. E. Little, S. T. Chu, T. Johnston, Y. Bromberg, L. Caspani, D. J. Moss, and R. Morandotti, *Science* **351**, 1176 (2016).
- [23] W. Asavanant, Y. Shiozawa, S. Yokoyama, B. Charoen-sombutamon, H. Emura, R. N. Alexander, S. Takeda, J. Yoshikawa, N. C. Menicucci, H. Yonezawa, and A. Furusawa, *Science* **366**, 373 (2019).
- [24] M. V. Larsen, X. Guo, C. R. Breum, J. S. Neergaard-Nielsen, and U. L. Andersen, *Science* **366**, 369 (2019).
- [25] X. Pan, S. Yu, Y. Zhou, K. Zhang, K. Zhang, S. Lv, S. Li, W. Wang, and J. Jing, *Phys. Rev. Lett.* **123**, 070506 (2019).
- [26] X. Su, S. Hao, X. Deng, L. Ma, M. Wang, X. Jia, C. Xie, and K. Peng, *Nat. Commun.* **4**, 2828 (2013).
- [27] S. Armstrong, M. Wang, R. Y. Teh, Q. Gong, Q. He, J. Janousek, H.-A. Bachor, M. D. Reid, and P. K. Lam, *Nat. Phys.* **11**, 167 (2015).
- [28] M. Pysher, Y. Miwa, R. Shahrokhshahi, R. Bloomer, and O. Pfister, *Phys. Rev. Lett.* **107**, 030505 (2011).
- [29] M. Chen, N. C. Menicucci, and O. Pfister, *Phys. Rev. Lett.* **112**, 120505 (2014).
- [30] J. Roslund, R. M. de Araújo, S. Jiang, C. Fabre, and N. Treps, *Nat. Photonics* **8**, 109 (2014).
- [31] F. A. S. Barbosa, A. S. Coelho, L. F. Muñoz-Martínez, L. Ortiz-Gutiérrez, A. S. Villar, P. Nussenzveig, and M. Martinelli, *Phys. Rev. Lett.* **121**, 073601 (2018).
- [32] J. Wang, J. Yang, I. M. Fazal, N. Ahmed, Y. Yan, H. Huang, Y. Ren, Y. Yue, S. Dolinar, M. Tur, and A. E. Willner, *Nat. Photonics* **6**, 488 (2012).
- [33] N. Bozinovic, Y. Yue, Y. Ren, M. Tur, P. Kristensen, H. Huang, A. E. Willner, and S. Ramachandran, *Science* **340**, 1545 (2013).
- [34] R. C. Devlin, A. Ambrosio, N. A. Rubin, J. B. Mueller, and F. Capasso, *Science* **358**, 896 (2017).
- [35] X. Wang, X. Cai, Z. Su, M. Chen, D. Wu, L. Li, N. Liu, C. Lu, and J.-W. Pan, *Nature (London)* **518**, 516 (2015).
- [36] T.-M. Zhao, Y. S. Ihn, and Y.-H. Kim, *Phys. Rev. Lett.* **122**, 123607 (2019).
- [37] Y. Zhang, M. Agnew, T. Roger, F. S. Roux, T. Konrad, D. Faccio, J. Leach, and A. Forbes, *Nat. Commun.* **8**, 632 (2017).
- [38] M. Lassen, G. Leuchs, and U. L. Andersen, *Phys. Rev. Lett.* **102**, 163602 (2009).
- [39] K. Liu, J. Guo, C. Cai, S. Guo, and J. Gao, *Phys. Rev. Lett.* **113**, 170501 (2014).
- [40] S. Li, X. Pan, Y. Ren, H. Liu, S. Yu, and J. Jing, *Phys. Rev. Lett.* **124**, 083605 (2020).
- [41] V. Boyer, A. M. Marino, and P. D. Lett, *Science* **321**, 544 (2008).
- [42] K. Zhang, W. Wang, S. Liu, X. Pan, J. Du, Y. Lou, S. Yu, S. Lv, N. Treps, C. Fabre, and J. Jing, *Phys. Rev. Lett.* **124**, 090501 (2020).
- [43] P. Gupta, R. W. Speirs, K. M. Jones, and P. D. Lett, *Opt. Express* **28**, 652 (2020).
- [44] A. S. Coelho, F. A. S. Barbosa, K. N. Cassemiro, A. S. Villar, M. Martinelli, and P. Nussenzveig, *Science* **326**, 823 (2009).
- [45] See Supplemental Material at <http://link.aps.org/supplemental/10.1103/PhysRevLett.125.140501> for measurement of covariance matrix and the verification of topological charges of output OAM modes, which includes Refs. [46–48].
- [46] A. Ya. Bekshaev, M. S. Soskin, and M. V. Vasnetsov, *J. Opt. Soc. Am. A* **20**, 1635 (2003).
- [47] P. Vafty, J. Banerji, and R. P. Singh, *Phys. Lett. A* **377**, 1154 (2013).
- [48] S. N. Alperin, R. D. Niederriter, J. T. Gopinath, and M. E. Siemens, *Opt. Lett.* **41**, 5019 (2016).
- [49] R. Simon, *Phys. Rev. Lett.* **84**, 2726 (2000).
- [50] R. F. Werner and M. M. Wolf, *Phys. Rev. Lett.* **86**, 3658 (2001).
- [51] G. Vidal and R. F. Werner, *Phys. Rev. A* **65**, 032314 (2002).
- [52] M. Krenn, R. Fickler, M. Fink, J. Handsteiner, M. Malik, T. Scheidl, R. Ursin, and A. Zeilinger, *New J. Phys.* **16**, 113028 (2014).
- [53] W. Zhang, L. Wang, W. Wang, and S. Zhao, *OSA Continuum* **2**, 3281 (2019).
- [54] N. C. Menicucci, S. T. Flammia, H. Zaidi, and O. Pfister, *Phys. Rev. A* **76**, 010302(R) (2007).
- [55] O. Pfister, *J. Phys. B* **53**, 012001 (2019).
- [56] N. C. Menicucci, S. T. Flammia, and O. Pfister, *Phys. Rev. Lett.* **101**, 130501 (2008).
- [57] P. Wang, M. Chen, N. C. Menicucci, and O. Pfister, *Phys. Rev. A* **90**, 032325 (2014).
- [58] H. Wang, C. Fabre, and J. Jing, *Phys. Rev. A* **95**, 051802(R) (2017).
- [59] C. K. Law and J. H. Eberly, *Phys. Rev. Lett.* **92**, 127903 (2004).
- [60] N. K. Fontaine, R. Ryf, H. Chen, D. T. Neilson, K. Kim, and J. Carpenter, *Nat. Commun.* **10**, 1865 (2019).
- [61] S. Tanzilli, A. Martin, F. Kaiser, M. P. De Micheli, O. Alibart, and D. B. Ostrowsky, *Laser Photonics Rev.* **6**, 115 (2012).
- [62] L. Caspani, C. Xiong, B. J. Eggleton, D. Bajoni, M. Liscidini, M. Galli, R. Morandotti, and D. J. Moss, *Light Sci. Appl.* **6**, e17100 (2017).
- [63] M. Kues, C. Reimer, J. M. Lukens, W. J. Munro, A. M. Weiner, D. J. Moss, and R. Morandotti, *Nat. Photonics* **13**, 170 (2019).
- [64] F. Lenzini, J. Janousek, O. Thearle, M. Villa, B. Haylock, S. Kasture, L. Cui, H.-P. Phan, D. V. Dao, H. Yonezawa, P. K. Lam, E. H. Huntington, and M. Lobino, *Sci. Adv.* **4**, eaat9331 (2018).